

Nonchaos-Mediated Mixed-Mode Oscillations in a Prey-Predator Model with Predator Dormancy

Joana G. Freire, Marcia R. Gallas and Jason A.C. Gallas

1 Introduction

A well-known property of ecosystems is that the equilibrium of the classical prey-predator system is destabilized when the carrying capacity, i.e., the environment maximal load, of the preys increases [1]. Under this circumstance, a Hopf bifurcation occurs. Its effect is to destabilize the coexistence of prey and predator in favor of a stable periodic cycle. Then, as the carrying capacity further increases, the amplitude of the periodic orbits also increase, with the minimum value of the population density decreasing. This dynamical interplay acts so that population extinction due to stochastic environmental perturbations becomes more likely. This is known as the paradox of enrichment [2]. However, this does not need to be the only scenario. As discussed by Kuwamura et al. [3], the extinction of populations is not always observed in natural enriched environments. In other words, the destabilization effect induced by eutrophication, namely the enrichment of the environment with nutrients,

J.G. Freire · M.R. Gallas · J.A.C. Gallas (✉)
Instituto de Altos Estudos da Paraíba, Rua Silvino Lopes 419-2502,
João Pessoa, PB 58039-190, Brazil
e-mail: jason.gallas@gmail.com

J.G. Freire
e-mail: negracarvao@gmail.com

M.R. Gallas
e-mail: marciagallas@gmail.com

J.G. Freire · M.R. Gallas · J.A.C. Gallas
Departamento de Física, Universidade Federal da Paraíba,
João Pessoa 58051-970, Brazil

J.G. Freire
Faculdade de Ciências, Instituto Dom Luiz, Universidade de Lisboa,
1749-016 Lisbon, Portugal

M.R. Gallas · J.A.C. Gallas
Complexity Sciences Center, 9225 Collins Ave. #1208,
Surfside, FL 33154-3046, USA

is somehow canceled in natural ecosystems. Many studies have attempted to clarify mechanisms for stabilizing the population dynamics in enriched environments. See, e.g., Refs. [3, 4] and several references therein.

This paper is motivated by a study of Kuwamura and Chiba [5] who proposed a mathematical framework to describe a stabilizing mechanism in enriched environment. The key idea of the approach is to consider the differentiation of the predator into active and dormant states. As indicated by a number of studies, dormancy of populations plays an important role in various biological studies [6–9]. According to Gyllström and Hansson [7], in comfortable environments zooplankton produces mainly subitaneous eggs. However, fertilized eggs (resting eggs, dormancy state) may be produced in order to escape periods of harsh environmental conditions. Experiments show [10] that the amplitude of prey-predator cycles of *Daphnia* and its algal prey in microcosms increases when a portion of ephippia-producing females is replaced by asexually-reproducing gravid females. This suggests that dormancy of predators may stabilize the population dynamics of *Daphnia* and its algal prey at high nutrient levels.

Kuwamura and Chiba [5] have shown that, under certain conditions, the dormancy of predators induces mixed-mode oscillations and chaos in the population dynamics of their prey-predator model. Using the theory of fast-slow systems, they argued mixed-mode oscillations and chaos to bifurcate from a coexisting equilibrium. These results are of interest because they may help to find experimental conditions under which one can demonstrate chaotic population dynamics in a simple phytoplankton-zooplankton (-resting eggs) community in a microcosm with a short duration.

The main finding reported here is the discovery of nonchaos-mediated cascades of mixed-mode oscillations observed in the prey-predator model with dormancy. Mixed-mode oscillations exist in two distinct flavors with easy to distinguish signatures [11]: Nonchaos-mediated cascades display *spike-adding sequences* while the more familiar chaos-mediated cascades involve *spikes-doubling sequences*. In contrast to the standard chaos-mediated cascades, the elusive nonchaos-mediated cascades were discovered quite recently and at present are known only for a handful of cases, namely, for an enzyme reaction [11, 12], for familiar models of oscillators [13, 14], and for a centrifugal flywheel governor system [15]. Thus, the observation of nonchaos-mediated cascades in the rather different context of a biological model adds one more example to the list above.

The present prey-predator model shares a sigmoidal function and other similarities with situations known to lead to very rich dynamics [16, 17]. However, its equations of motion also contain contributions from different terms, which are of interest for our on-going quest of classifying complexity phases in continuous-time dynamical systems [12, 18], so that a closer investigation seems warranted. This fact is another motivation for the present investigation. Before starting, recall that there are no theoretical methods capable of locating stability phases for motions of arbitrary periodicity, going beyond time-honored fixed-point analysis. Therefore, all such studies are necessarily of a numerical nature.

2 Prey-Predator Model with Predator Dormancy

The model of dormancy effects in the prey-predator population dynamics studied here is defined by a set of three coupled ordinary differential equations [3, 5]:

$$\frac{dp}{dt} = r \left(1 - \frac{p}{k}\right) p - f(p)z, \quad (1)$$

$$\frac{dz}{dt} = k_1 \mu(p) f(p)z + \alpha w - d_1 z, \quad (2)$$

$$\frac{dw}{dt} = \varepsilon [k_2 (1 - \mu(p)) f(p)z - \alpha w - d_2 w]. \quad (3)$$

Here, p and z denote population densities of prey and predators, respectively, and w is the population density of predators with a dormancy state (resting eggs). Parameters r and k correspond to the intrinsic growth rate and the carrying capacity of prey, respectively. The function $f(p)$, represents a positive strictly monotone increasing bounded function, taken to be a Holling type II functional response, namely $f(p) = bp/(c + p)$, where b and c represent the maximum foraging rate and the half saturation constant, respectively. Here, ε is a small time-scale separation parameter used to control the speed in the system [5]. Parameters k_1 and k_2 denote the growth rates of predators in the active and dormant states. The function $\mu(p)$ is a switching function which controls the induction of dormancy. It is given the sigmoidal function [16]

$$\mu(p) = \frac{1}{2} \left[\tanh \left(\frac{p - \eta}{\sigma} \right) + 1 \right], \quad (4)$$

where η and σ denote the switching level and the sharpness of the switching effect. This function implies that predators produce more resting eggs than subitaneous eggs when the prey density decreases below a certain level η . Parameters d_1 and d_2 denote the mortality rates of the active and dormant predators, respectively, while η is the hatching rate, i.e., resting eggs have a dormancy period with $1/\alpha$ on average. The model above is an extension of a prey-predator interaction-diffusion system based on the Bazykin model, known as the MacArthur-Rosenzweig model with intraspecific interaction (density-dependent inhibition) among predators, to which the effect of predator dormancy is incorporated. For details see Ref. [19].

Basically, Kuwamura and Chiba [5] considered two different situations of the model, $\varepsilon = 1$ and $\varepsilon = 0.2$, and studied how the bifurcation structure changes as a function k , the carrying capacity, and with variations of b and d_1 . Table 1 collects the default parameter values used here, unless stated otherwise.

Stability diagrams were constructed by integrating numerically Eqs. (1)–(3) using a standard fourth-order Runge-Kutta with fixed time-step $h = 0.01$. Such integrations were performed horizontally, from left to right, starting from an arbitrarily chosen initial condition, $(p, z, w) = (0.6, 0.15, 1.5)$, and proceeding by 'following the attractor' [17], namely by using the values stored in the computer buffers as initial conditions when incrementing parameters infinitesimally. The first 0.6×10^6

Table 1 Parameters values used here, taken from Ref. [5], in the same units

$r = 0.5$	$\alpha = 0.02$	$c = 2$	$\sigma = 0.1$	$b = 2$
$\eta = 1.0$	$d_1 = 0.2$	$d_2 = 0.0001$	$k_1 = 0.6$	$k_2 = 0.12$

integration steps were disregarded as a transient time needed to come close to the attractor, with an additional of 12×10^6 steps used to compute the Lyapunov spectrum (not presented in this paper). To find the number of peaks per a period, subsequently to the computation of Lyapunov exponents, integrations were continued for 12×10^6 additional time-steps, recording up to 800 extrema (maxima and minima) of the three variables and, from the recorded extrema, determining whether or not pulses repeated.

3 Nonchaos-Mediated Cascades of Mixed-Mode Oscillations

Figure 1 shows typical stability diagrams computed for the prey-predator system with dormancy, Eqs. (1)–(3). Such diagrams, called *isospike diagrams*, use a palette of 17 colors, as indicated by the colorbars, to display the number of spikes per period of the stable oscillations. Patterns with more than 17 peaks are plotted by recycling the 17 basic colors modulo 17. Black represents “chaos” (i.e., lack of numerically detectable periodicity), and white marks non-zero amplitude fixed-points (non-oscillatory solutions). The three diagrams on the top row in Fig. 1 display from left to right the number of spikes as observed by following the temporal evolution of the three variables, p , z , w , respectively. The next row shows magnifications of the regions inside the yellow boxes seen on the top panels.

Figure 1 shows a number of interesting facts. The three panels show the precise location where the number of spikes change for every variable. Oscillations in p and z display a much larger variation of their number of spikes then oscillations of w which display one spike over extended intervals when b increases. The vertical white stripes seen on the left of the panels show that, independently of b , the maximum foraging rate, the fixed-point is not affected by the carrying capacity k . There is a dynamical threshold for the effects of k to start to be noticed in the system. Furthermore, the onset of chaotic oscillations occurs only for specific ranges of b and k . In particular, the onset occurs for considerably larger values of k when b decreases.

Figure 2 shows a companion of two cascades of mixed-mode oscillations found in Eqs. (1)–(3), recorded the parallel lines seen in Fig. 1d and defined by the equations

$$b = -0.483k + 20.483 \quad \text{and} \quad b = -0.483k + 26.035. \quad (5)$$

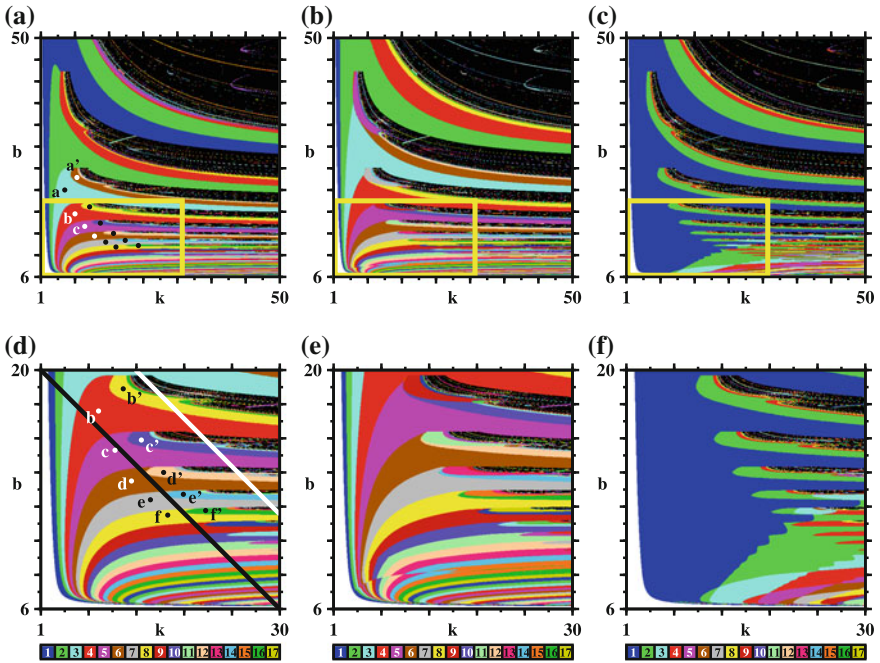


Fig. 1 Nonchaos-mediated cascades of mixed-mode oscillations, illustrated by sequences of domains not separated by chaos (shown in black), as a function of the maximum foraging rate b and the carrying capacity k . Panels (a)–(c) represent the number of spikes per period as measured for p , z , and w , respectively. The boxes in panels (a)–(c) are shown magnified in panels (d)–(f). The points marked in panels (a) and (d) are the same shown with more detail in Fig. 3, which is a magnification of panel (d). Bifurcations diagrams along the pair of lines in (d) are shown in Fig. 2. Here $\varepsilon = 0.2$ and other parameters as given in Table 1. Each individual panel displays the analysis of a mesh formed by 600×600 equally spaced parameter points

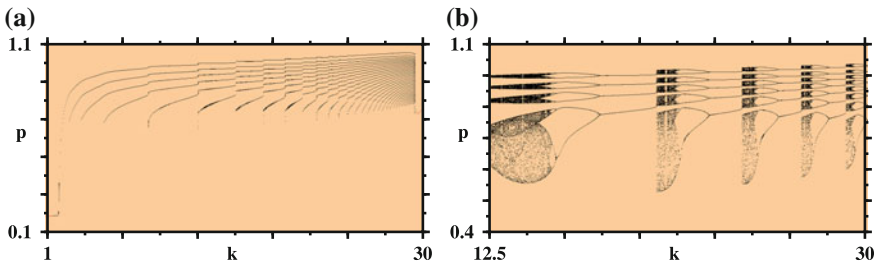


Fig. 2 Comparison of the rather distinct bifurcation diagrams underlying (a) nonchaos-mediated mixed-mode oscillations, and (b) the familiar chaos-mediated cascade. Panel (a) was recorded along the black line in Fig. 1d while (b) was recorded along the white line in the same figure. Nonchaos-mediated cascades display *spike-adding* sequences while chaos-mediated cascades show *spike-doubling*

The diagrams were obtained by starting from $(p, z, w) = (0.6, 0.15, 1.5)$ at the lowest value of k and proceeding by following the attractor until the highest k value. Figure 2a illustrates the new cascade of nonchaos-mediated mixed mode oscillations reported in this paper, while Fig. 2b shows an example of the chaos-mediated cascade found by Kuwamura and Chiba [5]. Both cascades look very different and reflect the distinct self-organization of oscillations seen in Fig. 1. Both cascades exist over relatively wide range of control parameters and, over limited intervals, may be even observed while varying just a single parameter, b , while keeping k fixed. Comparing Figs. 1d and 2b it is possible to recognize the existence of multistability: For instance, at the smallest values of k along the white line seen in Fig. 1d one sees the existence of period-3 solutions while the leftmost end of Fig. 2b displays chaos and no trace of period-3.

From Fig. 1d it is possible to recognize that the number of spikes increases by one as k grows along the black line. So, a natural question to ask is what exactly happens to the waveforms as they get more and more spikes continuously added to them. Figure 3 provides an answer. On the top panel of this figure one sees two sequences of points. The leftmost sequence, labeled by unprimed letters, corresponds to stability regions characterized by “primitive” number of spikes while points on the rightmost sequence, labeled with primed letters, lie inside domains where the number of spikes (not the period!) has doubled. The corresponding waveforms for every point in both sequences are shown under the stability diagram, while their coordinates, period, and number of spikes of their waveforms are collected in Table 2. In this Table, note that although the number of spikes doubles, the corresponding periods vary continuously, being not necessarily doubled. This lack of “period doubling” is a generic characteristic of continuous-time dynamical systems because the period varies *continuously* with parameters.

Figure 4 shows a remarkably complex “braided” self-organization of mixed-mode oscillations discovered for higher values of the carrying capacity k . In this region of the control parameter space one finds that the relatively regular sequences of nonchaos-mediated mixed-mode oscillations (seen in upper and lower portions of Fig. 4), are interrupted by a pair of stripes of chaos, represented in black in the diagrams. Between the stripes of chaos we find a braided sequence of domains arising from oscillations with a relatively high number of spikes per period.

The organization of oscillations between the stripes of chaos in Fig. 4 is magnified and illustrated in more detail in Fig. 5. In this figure, the phase diagram on the top contains points labeled by letters. It also contains numbers inside the upper and lower cascades of stability islands. Such numbers correspond to the number of spikes of the oscillations characteristic of each island. At about the center of the phase diagram there one sees four points labeled a, b, c, d , all of them lying inside the same oscillatory phase. As shown in the four panels in the lower part of Fig. 5, such points are all characterized by trains of periodic oscillations containing 38 spikes per period and, because $38 \bmod 17 = 4$, are represented with the color corresponding to 4 in

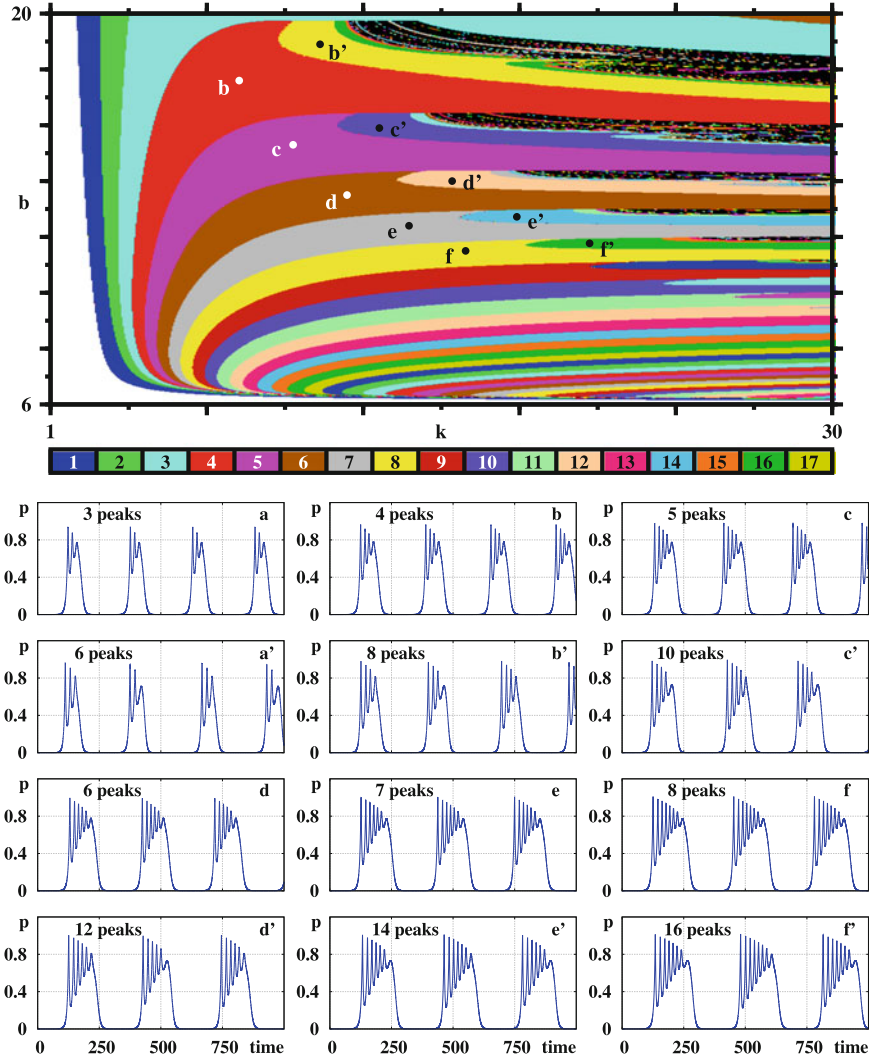


Fig. 3 Characteristic p waveforms along the nonchaos-mediated mixed-mode oscillation sequences indicated by the dots. Both sequences show cascades of spike additions and spike doublings. Here $\varepsilon = 0.2$. Evolutions start from the arbitrary initial condition $(p, z, w) = (0.6, 0.15, 1.5)$

Table 2 Characteristics of the oscillations for twelve time evolutions for $\varepsilon = 0.2$, shown in Fig. 3. Coordinates (k, b) , oscillation period, and number of peaks per period of the p oscillations

	k	b	Period	Peaks		k	b	Period	Peaks
a	5.9	22.0	253.02	3	a'	8.4	24.3	555.07	6
b	8	17.6	264.54	4	b'	11	18.9	570.85	8
c	10	15.3	280.71	5	c'	13.2	15.9	592.3	10
d	12	13.5	294.14	6	d'	15.9	14.0	619.96	12
e	14.3	12.4	311.59	7	e'	18.3	12.72	649.71	14
f	16.4	11.5	327.54	8	f'	21	11.77	681.35	16

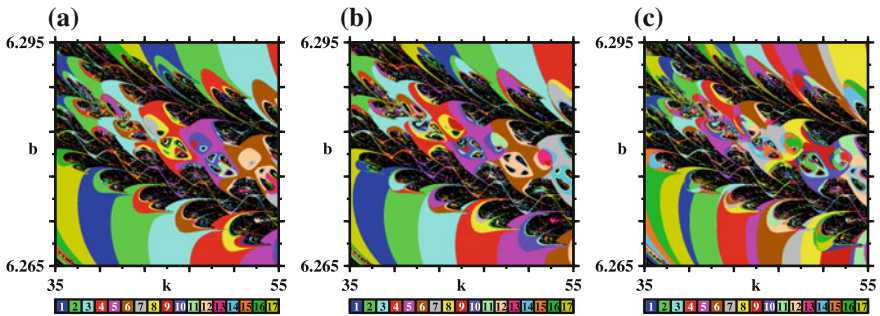


Fig. 4 Braided organization of mixed-mode oscillations, embedded between two stripes of chaos (in black), observed at higher values of the carrying capacity k . Panels (a)–(c) correspond to diagrams obtained by counting the number of spikes of p , z , and w , respectively. Details of these oscillations are given in Figs. 5 and 6. Here, $\varepsilon = 0.2$

the colorbar. From the four panels in Fig. 5 it is also possible to see that the period T of the oscillations increases clockwise, from point a to point d , inside the stability islands. The coordinates and characteristics for all points considered in Figs. 5 and 6 are given in Table 3.

Figures 5 and 6 show the time-evolution of the p variable. The other two variables show similar characteristics and, therefore, where not presented. The information recorded in Table 3 allow the time-evolution of the waveforms for all three variables to be easily recovered, if needed. An interesting point, however, is to clarify the nature of the reinjection loop responsible for starting every train of pulses shown in Figs. 5 and 6. As it is known, an important class of reinjection loops is associated with homoclinic bifurcations of a saddle-focus equilibrium state. In this case, the oscillatory part of the time-evolution corresponds to spiralling occurring essentially on a plane, with the reinjection happening perpendicular to it (see, e.g., Fig. 4 of Ref. [20]). Here, however, the spiralling occurs not on a plane but along a conical surface, as illustrated in Fig. 7. Furthermore, a close inspection of Fig. 7 reveals that the pair of spikes which appears between the pulse trains visible in Fig. 6 are responsible for a small loop that exists on the top of the cone in Fig. 7. We conjecture

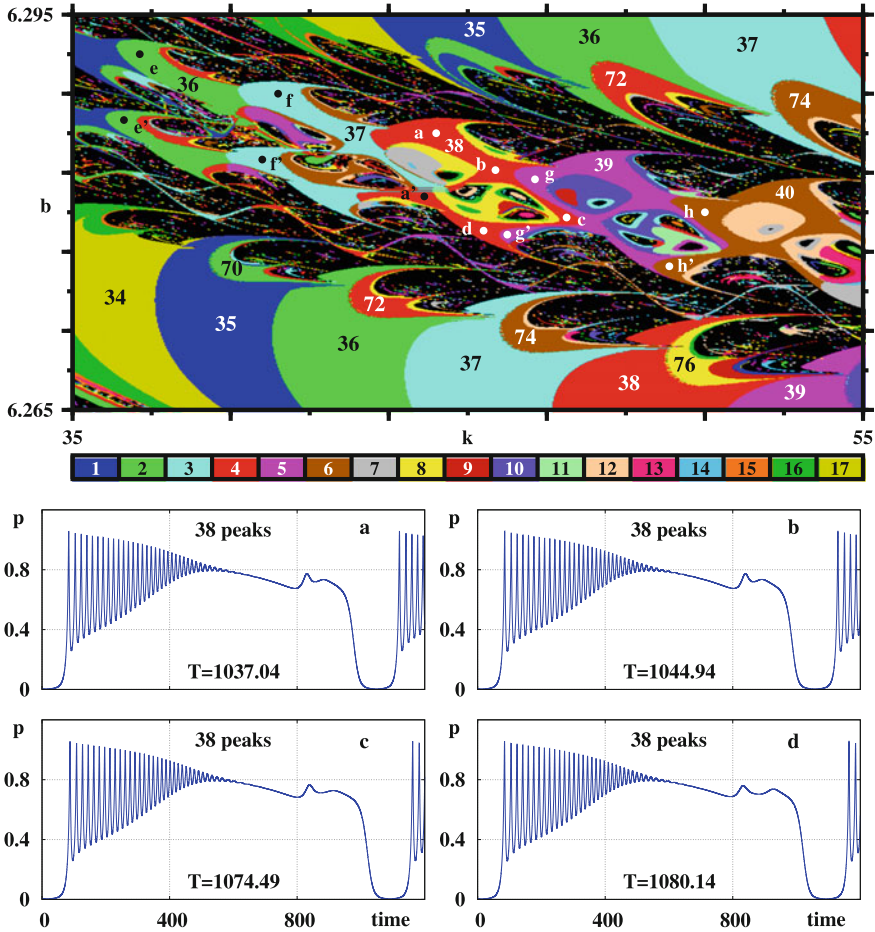


Fig. 5 Exceedingly complicated arrangement of periodic oscillations. Top panel: Magnification of Fig. 4a showing details of the braided organization found at higher values of the carrying capacity. Numbers indicate the number of spikes per period of the self-similar phases. The four bottom panels show how the waveform and period T of p pulses change when moving clockwise from points $a \rightarrow b, \rightarrow c, \rightarrow d$, defined in Table 3. Here, $\varepsilon = 0.2$. Evolutions start from $(p, z, w) = (0.6, 0.15, 1.5)$

that for other operation regimes of the model it should be possible to observe more complicated configurations in this region. We have not attempted to locate them since this requires investing considerable additional computer time.

So far, we discussed properties of nonchaos-mediated mixed-mode oscillations observed on the $k \times b$ control plane of the model. Is it possible to observe such oscillations in other control planes? Fig. 8 shows that it is not only possible to find them in other control planes but, in addition, that they exist over relatively wider parameter windows. In contrast to what was found in Fig. 1, note that the control-plane mosaic obtained by counting spikes of the w variable, Fig. 8c, is much different

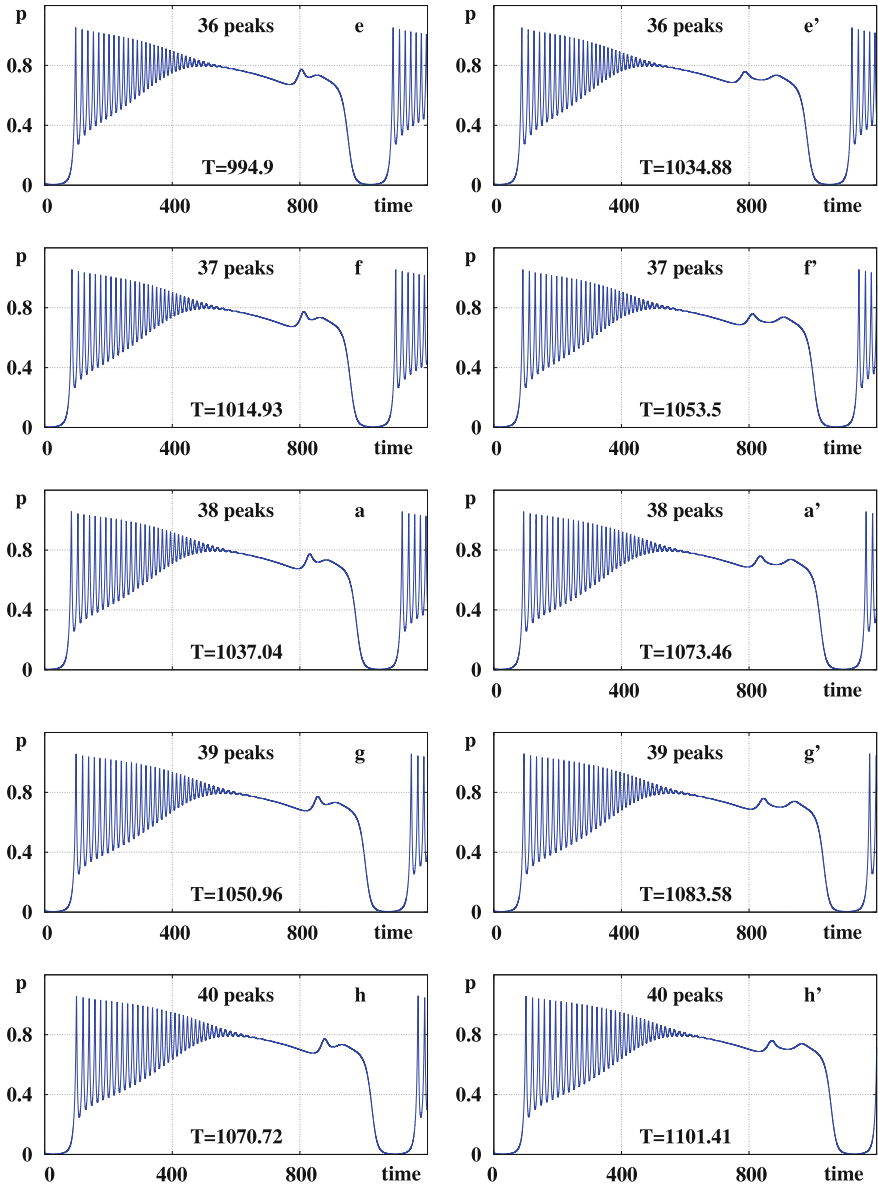


Fig. 6 Sequences of spike additions observed along the upper and lower parts of the braided structures in Fig. 5. Individual panels show the waveform of p for points labeled e, f, a, g, h and e', f', a', g', h' in Fig. 5. Note variations of the period T . All temporal evolutions start from the initial condition $(p, z, w) = (0.6, 0.15, 1.5)$

Table 3 Characteristics of the braided phases of periodic oscillations containing the points marked in Figs. 5 and 6. Coordinates (k , b), period T , and number of spikes per period of the p oscillations. Here, $\varepsilon = 0.2$

	k	b	Period	Peaks	k	b	Period	Peaks	k	b	Period	Peaks	
a	44.2	6.286	1037.04	38					a'	43.9	6.2812	1073.46	38
b	45.7	6.2832	1044.94	38	e	6.292	994.9	36	e'	36.3	6.287	1034.88	36
c	47.5	6.2796	1074.49	38	f	6.289	1014.93	37	f'	39.8	6.284	1053.5	37
d	45.4	6.2786	1080.14	38	g	6.2825	1050.96	39	g'	46	6.2783	1083.58	39
					h	6.28	1070.72	40	h'	50.1	6.2759	1101.41	40

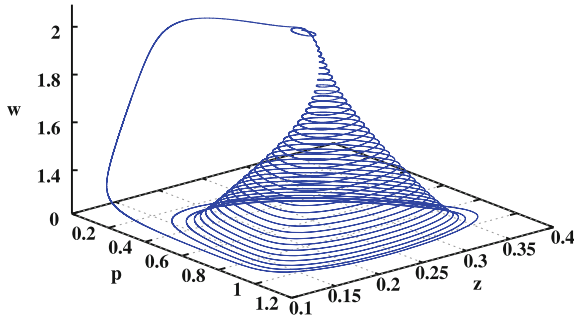


Fig. 7 Representation of the attractor corresponding to the point labeled *a* in Fig. 5, containing 38 spikes per period. The spiralling proceeds along a cone-like “witch hat” surface. All patterns in Figs. 5 and 6 produce similar *hats*

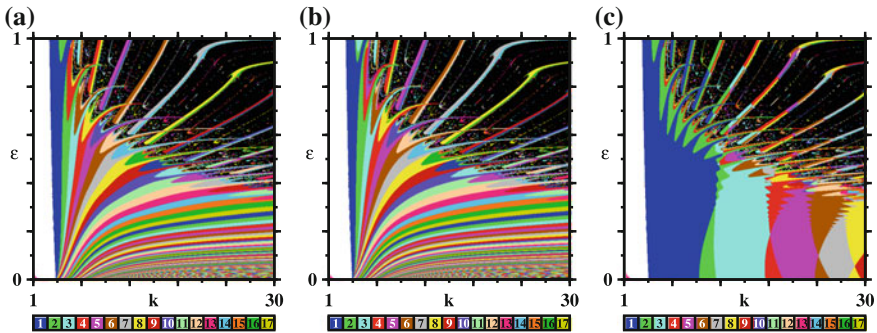


Fig. 8 Wide mosaics of nonchaos-mediated mixed-mode oscillations exist also on the $k \times \epsilon$ control plane. Panels (a)–(c) were obtained by counting spikes per period of p , z , w , respectively. Here, $b = 7$. Each panel displays the analysis of 600×600 parameter points

from the analogous mosaics obtained for variables p and z . We see no reason for nonchaos-mediated cascades of oscillations not to also exist for other combinations of parameters. However, a full exploration of all possible combinations is also a task demanding considerable additional computations.

4 Conclusions

This paper reported the discovery of abundant nonchaos-mediated sequences of oscillations, a novel and elusive type of mixed-mode oscillations, in an interesting prey-predator system including effects of predator dormancy, a strategy adopted in Nature to avoid extinction. As the carrying capacity increases, nonchaos-mediated sequences are found to appear well before the onset of chaos in the system, i.e., before the emergence of the more familiar chaos-mediated sequences. The observation of

nonchaos-mediated sequences in the system is of interest from a dynamical point of view because such sequences have been reported only recently and, at present time, are known to exist only for a small number of systems. As seen in Fig. 8 when $\varepsilon \rightarrow 0$, nonchaos-mediated display intricate accumulation limits, which remain to be investigated, particularly to understand the interplay between the fast and slow time-scales governing the system. In addition, as seen in Figs. 4, 5, and 8, stability phases emerge in control parameter space self-organized regularly but arranged in exceedingly complicated ways which are best described by graphical means than by words. It would be nice if the intricate variations predicted here could be observed in real-life measurements.

Acknowledgements JGF was supported by a postdoctoral fellowship (SFRH/BPD/101760/2014), from the FCT, Portugal. JACG was supported by CNPq, Brazil. All phase diagrams were computed on the CESUP-UFRGS Supercomputing Center located in Porto Alegre, Brazil.

References

1. Rosenzweig, M.L., MacArthur, R.H.: Graphical representation and stability conditions of predator-prey interactions. *Am. Nat.* **47**, 209–223 (1963)
2. Rosenzweig, M.L.: Paradox of enrichment: destabilization of exploitation ecosystems in ecological time. *Science* **171**, 385–387 (1971)
3. Kuwamura, M., Nakazawa, T., Ogawa, T.: A minimum model of prey-predator system with dormancy of predators and the paradox of enrichment. *J. Math. Biol.* **58**, 459–479 (2009)
4. Jensen, C.X.J., Ginzburg, L.R.: Paradox or theoretical failures? The jury is still out. *Ecol. Model.* **188**, 314 (2005)
5. Kuwamura, M., Chiba, H.: Mixed-mode oscillations and chaos in a prey-pradator system with dormancy of predators. *Chaos* **19**, 043121 (2009)
6. Alekseev, V., Lampert, W.: Maternal control of resting-egg production in *Daphnia*. *Nature* **414**, 899901 (2001)
7. Gyllström, M., Hansson, K.-A.: Dormancy in freshwater zooplankton: induction, termination and the importance of benthic-pelagic coupling. *Aquat. Sci.* **66**, 274295 (2004)
8. Hairston Jr., N.G., Hansen, A.M., Schaffner, W.R.: The effect of diapause emergence on the seasonal dynamics of a zooplankton assemblage. *Freshw. Biol.* **45**, 133145 (2000)
9. Ricci, C.: Dormancy patterns in rotifers. *Hydrobiologia* **446**, 111 (2001)
10. McCauley, E., Nisbet, R.M., Murdoch, W.W., de Roos, A.M., Gurney, W.S.C.: Large-amplitude cycles of *Daphnia* and its algal prey in enriched environments. *Nature* **402**, 653656 (1999)
11. Hauser, M.J.B., Gallas, J.A.C.: Nonchaos-mediated mixed-mode oscillations in an enzyme reaction system. *J. Phys. Chem. Lett.* **5**, 4187–4193 (2014)
12. Gallas, M.R., Gallas, J.A.C.: Nested arithmetic progressions of oscillatory phases in Olsen's enzyme reaction model. *Chaos* **25**, 064603 (2015)
13. Freire, J.G., Gallas, M.R., Gallas, J.A.C.: Chaos-free oscillations. *Europhys. Lett.* **118**, 38003 (2017)
14. Freire, J.G., Gallas, M.R., Gallas, J.A.C.: Stability mosaics in a forced Brusselator: auto-organization of oscillations in control parameter space. *Eur. Phys. J. Spec. Top.* **226**, 1987–1995 (2017)
15. Rao, X., Chu, Y., Lu-Xu, Y., Chang, Z., Zhang, J.: Fractal structures in centrifugal flywheel governor system. *Commun. Nonlinear Sci. Numer. Simul.* **50**, 330339 (2017)
16. Freire, J.G., Pöschel, T., Gallas, J.A.C.: Stern-Brocot trees in spiking and bursting of sigmoidal maps. *Europhys. Lett.* **100**, 48002 (2012)

17. Freire, J.G., Field, R.J., Gallas, J.A.C.: Relative abundance and structure of chaotic behavior: the nonpolynomial Belousov Zhabotinsky reaction kinetics. *J. Chem. Phys.* **131**, 044105 (2009)
18. Gallas, J.A.C.: Spiking systematics in some CO₂ laser models. *Adv. Atom. Mol. Opt. Phys.* **65**, 127–191 (2016)
19. Kuwamura, M.: Turing instabilities in prey-predator systems with dormancy of predators. *J. Math. Biol.* **71**, 125–149 (2015)
20. Vitolo, R., Glendinning, P., Gallas, J.A.C.: Global structure of periodicity hubs in Lyapunov phase diagrams of dissipative flows. *Phys. Rev. E* **84**, 016216 (2011)